

Atmospheric Ice Crystals over the Antarctic Plateau in Winter

VON P. WALDEN

Department of Geography, University of Idaho, Moscow, Idaho

STEPHEN G. WARREN AND ELIZABETH TUTTLE*

Department of Atmospheric Sciences, University of Washington, Seattle, Washington

(Manuscript received 16 July 2002, in final form 19 April 2003)

ABSTRACT

Falling ice crystals were collected daily on a gridded glass slide at South Pole Station, Antarctica, during the Antarctic winter of 1992 and were photographed through a microscope. Nine types of ice crystals are identified, which fall into three main categories: "diamond dust," blowing snow, and snow grains. The dimensions of about 20 000 crystals were measured on scanned images of the photomicrographs. The predominant crystal types are hexagonal columns and plates (diamond dust) and rounded particles of blowing snow. Diamond-dust crystals have a large range of lengths (2–1000 μm) and aspect ratios (0.1–100). Diamond-dust crystals can usually be classified as either columns or plates; nearly equidimensional crystals are rare. "Long prism" crystals with aspect ratios greater than 5 were collected often, and very long prisms ("Shimizu" crystals), 1000 μm long but only 10 μm thick, were collected occasionally. The extreme Shimizu crystals were predominant on only one winter day, but the meteorological conditions on that day were not unusual. Some precipitation was observed on every day; even when the dominant crystal type was blowing snow, there were always, in addition, some snow grains or diamond dust. Blowing-snow particles dominate by number and contribute nearly one-half of the total surface area. Bullet clusters and blowing snow each contribute about one-third of the total volume of atmospheric ice. Size distributions of the equivalent spherical radius are obtained for each of the nine crystal types, as well as for the three main categories of crystals, using the volume-to-area ratio to specify the equivalent spheres. In addition, the effective radius for each day when crystals were sampled is computed. Many of the distributions are approximately lognormal. The effective radius (area-weighted mean radius) of the entire size distribution of diamond dust is 12 μm in winter, somewhat smaller than in summer (15 μm). The small size of wintertime blowing snow allows it to reach heights of tens of meters in winter, as compared with only a few meters in summer. The average effective radius was 11 μm for blowing snow and 24 μm for snow grains. The most probable effective radius for any given day in winter is about 11 μm .

1. Introduction

Ice crystals are nearly always present in the atmospheric boundary layer over the Antarctic Plateau. They interact with both solar and infrared radiation and, therefore, affect the planetary energy budget. Regional and general circulation models are sensitive to the shapes and sizes of ice crystals and water droplets specified for antarctic clouds (Lubin et al. 1998).

It has been difficult to retrieve properties of clouds over snow using satellite instruments, such as the Advanced Very High Resolution Radiometer (AVHRR). With new instruments becoming available, such as the Moderate Resolution Imaging Spectroradiometer

(MODIS) and the Atmospheric Infrared Sounder (AIRS), more information should be retrievable, and it will be essential to have in situ data with which to evaluate the retrievals.

Knowledge of atmospheric ice crystals is also important for remote sensing of the surface. The Geoscience Laser Altimeter System (GLAS) (Schutz 1998) will use satelliteborne visible and infrared lasers to monitor the height of the Antarctic Ice Sheet for assessment of its mass balance. Thin ice clouds adjacent to the surface will affect the timing of the returned signal (J. D. Spinhirne 1999, personal communication) and, thus, the accuracy of the retrieved height.

Throughout the 6-month winter (April–September) on the Antarctic Plateau, a strong surface-based temperature inversion persists. Vertical mixing within this layer, which may be facilitated by horizontal winds flowing over the rough snow surface, causes the boundary layer air to become supersaturated with respect to ice, so that small ice crystals, called "diamond dust,"

* Current affiliation: Antioch University, Seattle, Washington.

Corresponding author address: Von P. Walden, Dept. of Geography, University of Idaho, Moscow, ID 83844-3021.
E-mail: vonw@uidaho.edu

TABLE 1. Frequency of occurrence of diamond dust, blowing snow, and snow grains in the wintertime (Apr–Sep) at South Pole Station. Values are derived from visual observations made every 6 h by the South Pole Weather Office. The data from 1991 were judged unreliable and, therefore, not used. The column entitled “Crystals absent” represents the percent of days when neither ice crystals, blowing snow, nor snow grains are present.

Year	Frequency of occurrence (%)			
	Crystals absent	Diamond dust	Blowing snow	Snow grains
1989	4	85	35	2
1990	16	45	36	6
1991	—	—	—	—
1992	8	58	35	12
1993	6	76	25	9
1994	7	65	50	7
1995	12	51	53	7
6-yr average	9	63	39	7

form in the inversion layer. Longwave cooling of the near-surface air can also lead to supersaturation and ice-crystal formation, even in the absence of mixing. Longwave radiation from clouds aloft can weaken the inversion, but cannot destroy it completely, so diamond dust often forms even under clouds.

Table 1 shows the frequencies of occurrence of the three major types of wintertime ice crystals reported at South Pole Station, Antarctica, in six different years. Crystals are absent in the near-surface atmosphere about 9% of the time in winter. In contrast, diamond dust is reported about 63% of the time, and blowing snow about 39%. Because they are both quite common and often occur together, the sum of their frequencies of occurrence may exceed 100%. In fact, our photographs indicate that both diamond dust and blowing snow occur more frequently than reported by the weather office; in every photo of blowing snow there were also some diamond-dust crystals, and in some cases where the weather office reported only diamond dust because of weak winds, we observed residual blowing snow as well.

Larger snow grains, falling from clouds, are reported much less often (7%), but nonprecipitating clouds are common; the average cloud cover in winter is about 40% (Hahn et al. 1995, their Fig. 13b).

There have been several previous studies of ice-crystal precipitation on the Antarctic Plateau. Hogan (1975) and Kikuchi and Hogan (1979) reported that summertime ice-crystal precipitation at the South Pole consists primarily of columns, bullets, clusters of bullets, and small diamond-dust particles (columns, pyramids, and hexagonal plates). They reported that diamond dust can form by homogeneous nucleation at temperatures below -40°C in atmospheric layers near the surface that are supersaturated with respect to ice, under otherwise clear skies. At temperatures above -40°C , larger particles are precipitated from clouds, or, possibly, grow as a result of seeding from overlying clouds. Ohtake (1978) sug-

gested that summertime ice-crystal precipitation at the South Pole is generated within three atmospheric layers: clusters of bullets in high cirrus clouds; large plates and columns, as well as bullets, in midlevel altostratus clouds; and small crystals in the lowest 1 km. Ohtake and Yogi (1979) classified Antarctic wintertime ice-crystal precipitation into six categories. These included large clusters of bullets (1 mm or larger), bullets and columns on the order of 1 mm in length, thin hexagonal plates and columns ($200\ \mu\text{m}$ or less), and smaller crystals of various shapes: “pencil,” triangular, block, and polyhedral. Shimizu (1963) observed “long prism” crystals in winter at Byrd Station (80°S , 120°W), which have a large aspect ratio ($c/2a > 5$, see Table 2 for definitions of c and a).

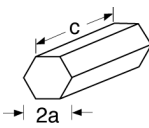
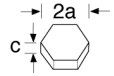
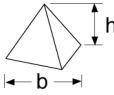
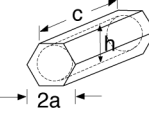
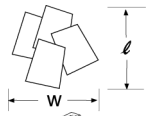
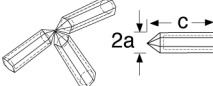
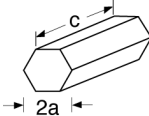
Size distributions of Antarctic ice crystals in winter and spring were reported by Smiley et al. (1980), but only for particles larger than $50\ \mu\text{m}$. They observed the same ice-crystal shapes reported earlier. Their reported size distributions most likely represent the largest crystal dimension: c axis for columns and a axis for plates.

Observations have also been made on the coast at Syowa Station (69°S , 40°E). Kikuchi (1972) observed “sintered frozen cloud particles.” We observed only 10 of these crystals during the winter of 1992 and, therefore, this crystal type is not considered here. Hatanaka et al. (1999) reported size distributions of snow particles at Syowa, but only for particles with radii greater than $100\ \mu\text{m}$.

Near-surface ice crystals in the Antarctic are quite different from those observed in the Arctic. More pristine crystal shapes are observed in the Antarctic (Tape 1994) than in the Arctic (Korolev et al. 1999), yielding spectacular haloes. Asuma et al. (2000) photographed precipitating ice crystals at the surface in the Arctic and reported much larger particles than those observed over the Antarctic Plateau, presumably because of the greater availability of moisture in the Arctic. Blanchet and Girard (1994) have speculated that diamond-dust ice crystals near the surface in the Arctic are important contributors to the surface energy and moisture budgets. Girard and Blanchet (2001a,b) have recently attempted to model near-surface ice crystals in the Arctic.

Here we present information on the shapes and sizes of wintertime ice crystals over South Pole Station. Section 2 describes the observations and methods used to process the photomicrographs. That section also describes the relative frequencies of different types of crystals and their average surface area and volume. Section 3 reports on the measurements and size distributions of the different crystal types, as well as their effective radii. The distribution of daily average effective radii is also given. Section 4 discusses the lack of correlation of particle size with boundary layer meteorological conditions. Section 5 discusses the occurrence and effects of diamond dust and blowing snow.

TABLE 2. Types of crystals that were identified and sized from the photomicrographs; n is the number of bullets in a cluster.

Crystal type	No. sized	Shape	Dimension (μm)			
			Min	Max	Mean	
Diamond dust						
Solid columns	2381		$2a$ c	2 7	49 1006	13 61
Plates	2127		$2a$ c	4 3	158 103	27 13
Pyramids	95		b h	13 9	57 48	29 22
Hollow columns	21		$2a$ c h	8 31 4	34 208 21	16 85 9
Blowing snow						
Blowing snow	12 958		$2a$ $2b$	4 3	130 97	19 15
Residual blowing snow	2411		$2a$ $2b$	7 4	127 56	21 16
Snow grains						
Sector plate clusters	160		l w	49 40	831 456	196 136
Bullet clusters	67		$2a$ c n	19 55 1	284 959 16	84 243 4
Snow grain columns	24		$2a$ c	35 90	201 372	94 193

2. Observations

From late June to the end of September 1992, a gridded microscope slide was placed on an elevated platform on the roof of the Clean Air Facility at South Pole Station and was allowed to collect ice crystals. The ice crystals fell naturally onto the uncoated slide, which was scribed with grid lines with spacings of $50 \mu\text{m}$. The average collection time was about 3 h, but ranged from 30 min to 6 h. Figure 1 shows that the slide was exposed long enough to adequately sample the falling crystals. The sloping contours show the minimum time required to sample a single crystal as a function of concentration in the air and the terminal velocity. The terminal velocities for different types of Antarctic ice crys-

tals are also shown as vertical dashed lines. [These velocities were calculated using equations from section 10.4 of Pruppacher and Klett (1978) with the average, measured dimensions of the different crystal types (see section 3 and Table 2)]. The letters on those lines designate the concentrations necessary to collect a single crystal over the average collection time of 3 h on the area of the microscope slide (3.37 mm^2). [A range of typical concentrations for cirrus clouds (Chen et al. 1997) is shown for reference as the gray area.] Due to the low values of the minimum concentration necessary to sample the various crystal types, we probably did not miss any significant types of crystals.

In strong winds, large crystals were blown off the

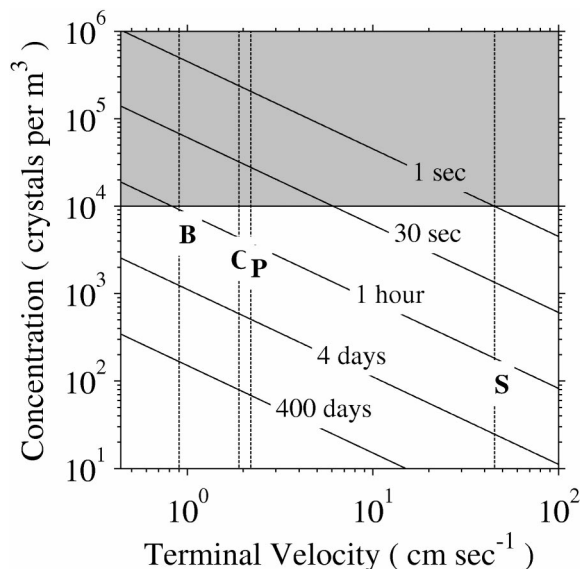


FIG. 1. Contour plot showing the time needed to collect a single ice crystal on the photographed region of the microscope slide (area = 3.37 mm²) as a function of the number concentration and terminal velocity of the crystals. The vertical dashed lines are estimates of the terminal velocities of typical blowing snow (B), diamond-dust columns (C) and plates (P), and large snow-grain columns (S). The terminal velocities were calculated using the average dimensions of these crystal types from Table 2. The position of the letters along the dashed lines designate the minimum concentrations necessary to collect one crystal, assuming a collection time of 3 h. For reference, the gray area at large concentrations shows typical values of crystal concentrations in cirrus clouds from Chen et al. (1997).

gridded platform of the microscope slide and were collected in troughs on the side of the platform, while small crystals stuck to the grid. On the few occasions when this occurred, the larger crystals were photographed in the trough rather than on the platform, and were sized using the magnification factor from another image.

After exposure to the atmosphere, the slide was taken to an unheated vestibule where the microscope was kept; the temperature of the microscope was typically -40°C . A Nikon F3 camera with Kodak TMAX 100 black-and-white film was attached to the microscope to photograph the gridded slide.

For this study, we used 84 images, and measured over 20 000 ice crystals. The images represent an adequate sample of wintertime ice crystals over the Antarctic Plateau, because they were obtained under all types of meteorological conditions throughout the winter. The images were photographed between the dates of 28 June 1992 and 30 September 1992, at surface air temperatures ranging from -73° to -35°C . For these months, meteorological data are available from the South Pole Weather Office (SPWO), including surface measurements of temperature, pressure, wind speed and direction, visual surface observations of sky conditions, and temperature profiles from daily radiosondes.

The photographs were digitized using an electronic scanner at 300 dots per inch (dpi) and were stored as

tagged image format file (TIFF) images. The image-viewing program, xv, in conjunction with the image-processing workbench, IPW, were used to size the ice crystals on a UNIX workstation (information available online at <http://www.ices.ucsb.edu/~ipw2/>). The images were displayed by xv, while IPW allowed the user to draw a vector over the image. The x - y positions of the endpoints of the vector, in pixels, were stored in a text file. The length of the vector was determined by applying an appropriate scale factor, converting pixels to micrometers. The scale factor was determined by drawing a vector between grid lines of known separation on the slide.

The uncertainty in sizing ice crystals was estimated by repeatedly measuring the distance between various grid lines on a few representative images. The mean and standard deviation of 30 measurements between two scribe lines spaced 50 μm apart (low-magnification image) are 67.3 ± 1.2 pixels. For scribe lines spaced 200 μm apart, the mean and standard deviation are 270.5 ± 1.1 pixels. This yields a scale factor of $50/67.3 = 200/270.5 = 0.74 \mu\text{m}$ per pixel and a distance-measurement uncertainty of less than 1 μm . The uncertainty in the distance between two closely spaced lines of unknown separation distance (about 5.5 μm) was also determined as about 1.2 pixels, indicating that the sizing uncertainty is independent of distance over most of the range of sizes of interest, 1–1000 μm . It was possible to reduce the sizing uncertainty somewhat by zooming into the crystals being sized, but this approach was not pursued because of the excessive time required. The digitization resolution of 300 dpi was chosen because it gave adequate sizing accuracy, while keeping the digital images to a manageable size.

3. Methods

a. Classification of ice-crystal shapes

Table 2 shows the nine types of ice crystals identified in the images and the number of crystals that were sized of each type. Each crystal type requires at least one dimension for its description, but some require as many as three. These dimensions are illustrated in the sketches in Table 2. Bullet clusters have, in addition, a value n that designates the number of crystals in the cluster. Table 3 shows the relative frequency of occurrence of the different ice-crystal types. Also shown in Table 3 are the relative contributions of each crystal type to the total surface area and total volume. All three quantities were obtained by dividing the number of crystals on each photomicrograph by the slide exposure time and also by accounting for the different areas photographed, depending on the magnification used. Table 4 lists the assumptions made in sizing the different types of ice crystals.

The crystals can be separated into three major categories: diamond dust, blowing snow, and snow grains.

TABLE 3. Relative frequency of occurrence of the different ice-crystal types from the South Pole 1992 photomicrographs, as well as the relative contributions to the total surface area and total volume. The values in boldface type are the maximum values.

Crystal type	Relative frequency (%)	Contribution to total surface area (%)	Contribution to the total volume (%)
Diamond dust			
Solid columns	10	15	7
Plates	9	12	9
Pyramids	<1	<1	<1
Hollow columns	<1	<1	<1
Blowing snow			
Blowing snow	72	46	31
Residual blowing snow	8	6	5
Snow grains			
Sector-plate clusters	<1	8	5
Bullet clusters	<1	11	39
Snow-grain columns	<1	1	3

Figure 2 shows five examples of photomicrographs of ice crystals; the grid lines on the microscope slide are visible in each image. For reference, Fig. 3 displays the temperature profiles obtained by the SPWO that were nearest to the time period over which the crystals were sampled. Each crystal is classified into one of the three major categories based on its size and shape. Diamond dust and snow grains are distinguished from blowing snow by their shape; diamond dust and snow grains have crystalline shapes, while blowing snow are rounded particles. Diamond-dust crystals are distinguished from snow grains by size—primarily thickness. Figure 2b shows examples of all three of the major crystal categories. The small, rounded crystals are blowing snow, the bullet clusters are snow grains, and there are both long and short columns of diamond dust.

1) DIAMOND DUST

Figure 2a shows a sample of diamond-dust ice crystals, consisting of both columns and plates. Figure 2e shows hexagonal columns with large aspect ratios, called Shimizu crystals (see section 3). Columns are designated as either solid or hollow; however, many “solid” columns have small inclusions of air. To be classified as a hollow column, we required that the inclusion be greater than 50% of the length of the column. The plates observed by Kikuchi and Hogan (1979) in summer were of many different shapes, including hexagonal, pentagonal, trapezoidal, triangular, and rhomboidal. Almost all of the plates we collected in winter were hexagonal; however, the six sides were often unequal. In the past (Kobayashi 1958, 1967; Fletcher 1970, his Fig. 5.7), it was thought that only columnar crystals could form below about -28°C . However, both the columns and plates in Fig. 2d must have formed at tem-

TABLE 4. Assumptions made in sizing the ice crystals.

Ice-crystal type	Sizing assumption
Diamond dust	
Plates	The <i>c</i> axes for plates where only the <i>a</i> axis was measurable are based on the aspect ratios for all plates where both the <i>a</i> and <i>c</i> axes were measurable.
Pyramids	For calculating surface area and volume, pyramids are right circular cones.
Hollow columns	The hollow portion of the crystal is 75% of the <i>c</i> -axis length. The hollow portion in the <i>a</i> -axis direction is measured directly. The inside surface area of a hollow column is accounted for by addition to the outside surface area; the inside empty volume is subtracted.
Blowing snow	
Blowing-snow clusters	Clusters of blowing-snow particles are categorized as blowing snow. All particles within a blowing-snow cluster are the same size as the single particle that was actually sized. To account for “necking” between crystals, the actual photographs were examined to decide on an appropriate fractional reduction of surface area. The photographs suggest that there is a range of values for the necking fraction (f_n) from crystals that are barely touching ($f_n = 0$) to those that have their entire cross section connected ($f_n = \pi R^2$). However, the majority have a necking fraction for which about two-thirds of their cross section is necked, which is equal to 1/6 of the surface area in the case of spheres. Necking does not affect the volume.
Snow grains	
Sector-plate clusters	The individual plates are rectangular. There are six plates in a sector-plate cluster. The thickness of each plate is $10\ \mu\text{m}$. The dimensions of each plate are one-third the size of the cluster (see Table 2).
Bullet clusters	All columns within a bullet cluster are the same size as the single bullet that is actually sized. Each bullet in a bullet cluster is hollow; this was justified by inspection of all the photos containing bullet clusters. The hollow portion of the bullet is 75% of both the <i>a</i> - and <i>c</i> -axis lengths, which yields a wall thickness between 5 and $15\ \mu\text{m}$.

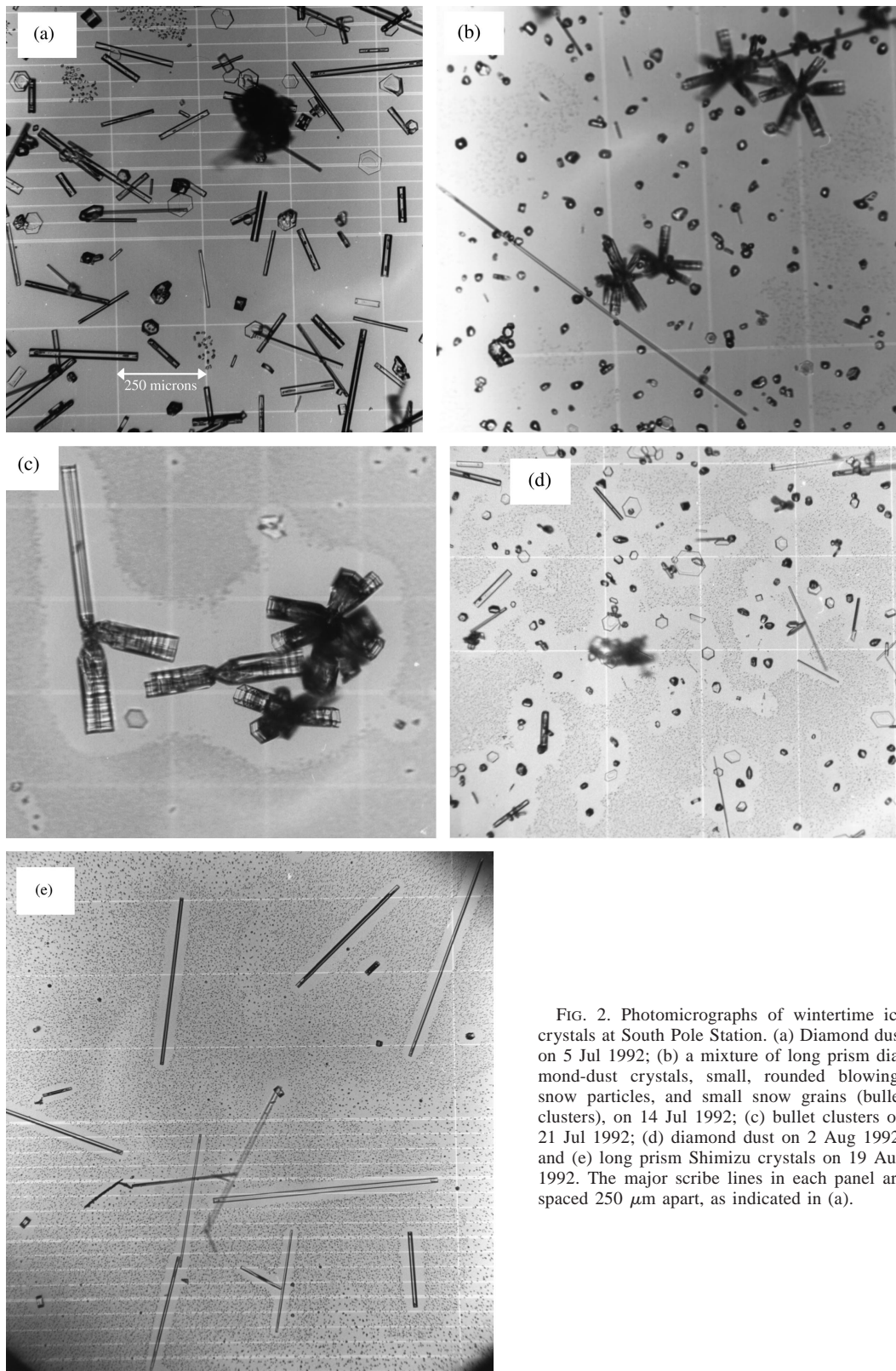


FIG. 2. Photomicrographs of wintertime ice crystals at South Pole Station. (a) Diamond dust on 5 Jul 1992; (b) a mixture of long prism diamond-dust crystals, small, rounded blowing-snow particles, and small snow grains (bullet clusters), on 14 Jul 1992; (c) bullet clusters on 21 Jul 1992; (d) diamond dust on 2 Aug 1992; and (e) long prism Shimizu crystals on 19 Aug 1992. The major scribe lines in each panel are spaced $250 \mu\text{m}$ apart, as indicated in (a).

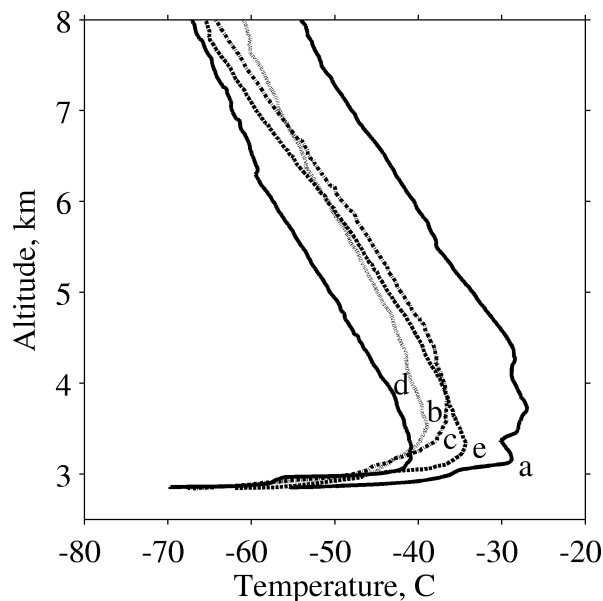


FIG. 3. Radiosonde temperature profiles for the days in Fig. 2 on which ice crystals were sampled. The letter just to the right of each line designates the particular image in Fig. 2 that the profile represents; profile "a" from 5 Jul 1992 represents Fig. 1a. Profile "d" (2 Aug 1992) is for one of the coldest days of the winter (surface temperature -70°C). The surface elevation at South Pole Station is 2.8 km. All profiles have been corrected for thermal lag of the thermistor on a rapidly rising sonde (Mahesh et al. 1997).

peratures below -40°C , the highest temperature in the tropopause on that day (Fig. 3).

Plates may have either one or two measurable dimensions. As crystals fall through air, they tend to orient themselves such that their surface area is maximized perpendicular to the direction of motion. In the case of hexagonal plates, the large axis (a axis) is oriented roughly perpendicular to the direction of motion. Therefore, plates normally settle onto the microscope slide with their a -axis face (plate face) horizontal, exposing only that one dimension for measurement. However, some plates settled obliquely such that both a and c axes were visible, usually because they fell onto the side of another crystal, which allows both dimensions to be measured. It is possible that plates with large aspect ratios were more likely to land on their sides. If so, the aspect ratios we obtain for plates are biased high.

The aspect ratios ($c/2a$) of the plates with two measurable dimensions were used to estimate the c axes of the other plates, based on the lengths of their a axes. This was accomplished by first determining the geometric mean and standard deviation of the aspect ratios (Reist 1993) for the plates with both measured dimensions; the distribution of aspect ratios is approximately lognormal. Then, a series of random aspect ratios were generated, having this same geometric mean and standard deviation. These aspect ratios, randomly chosen, were multiplied by the values of $2a$ for the plates with one measurable dimension to assign their c values.

2) BLOWING SNOW

Figures 2b and 2d show examples of blowing-snow particles. They are created when the surface wind is sufficiently strong to lift ice crystals off the surface; the threshold wind speed is about 7 m s^{-1} . The process is assisted by saltation, in which a precipitating crystal or a falling blowing-snow particle dislodges a surface grain (Schmidt 1982). During the process of being lofted into the air, the crystals undergo collisions that break them apart. The jagged edges of broken crystals become rounded quickly, not only by additional collisions, but also by selective sublimation of the sharper convex corners. Therefore, blowing-snow particles no longer retain any resemblance to the hexagonal structure of precipitation crystals and are represented here as spheroids. Spheroids are ellipsoids in which two of the three axes are equal. Blowing-snow particles seem to satisfy this restriction, so we report only two dimensions for each particle. In any case, the blowing-snow particles are usually nearly spherical. Blowing-snow particles collected on the microscope slide were often clustered. These clusters may form in the atmosphere or on the collection slide; they typically contained 10 individual spheroidal particles in a branched pattern. The noncompact nature of the clusters suggests that their radiative properties and fall speeds are similar to those of the individual spheroids. In this paper, it is the individual elements of a cluster that are sized, counted, and analyzed, not the cluster as a whole.

Residual blowing-snow particles are similar to blowing-snow particles in size and shape, but were collected on days when winds were insufficient to initiate blowing snow. If the wind speed was less than 13 kn (6.7 m s^{-1}), the weather observers normally did not report blowing snow because of insufficient wind; but, we observed that blowing snow (identified by crystal shape) continued to settle for a day or two after the winds had weakened. The average wind speed was 4.5 m s^{-1} on days when residual blowing snow was collected, and 7.5 m s^{-1} on days when blowing snow was reported by the weather observers.

3) SNOW GRAINS

Snow grains are ice crystals precipitated from clouds. They are usually sector-plate clusters, bullet clusters, or snow-grain columns. Examples of bullet clusters are seen in Figs. 2b and 2c. They are usually much larger than either diamond-dust or blowing-snow particles due to the relatively large source of moisture within the cloud. Snow grains represent only 1% of the crystals, but are responsible for 20% of the total crystal area and 47% of the total volume (Table 3). Sector-plate clusters are the most common type of snow grain. Visual examination of all of the images of bullet clusters showed that the individual bullets within a cluster were always hollow throughout the entire winter. This gives them a

small effective radius, approximately half the width of one wall of one bullet, because the interior surfaces can also scatter light.

4) ARTIFACTS

The small patches of tiny equidimensional ice particles (1–3 μm) seen in all five frames of Fig. 2 are believed to be crystals created by humidity from the photographer, even though precautions were taken to not breathe on, or otherwise disturb, the microscope slide during the photomicrography. Some of these small crystals were cannibalized by the larger natural crystals nearby through vapor diffusion before the photograph was taken. By estimating the total volume of the cannibalized crystals and then comparing it to the volume of a natural crystal, it is shown that this process causes the natural crystal to grow by at most 10% in volume (3% in any linear dimension).

The predominant crystal types are diamond-dust columns, diamond-dust plates, and blowing snow. Precipitation seems to be forming continuously throughout the winter. Every time the microscope slide was set out, some crystals of falling snow (diamond dust or snow grains) were always collected. Even when the dominant crystal type was blowing snow, there was always some falling snow as well.

b. Effective radius

The crystal dimensions are used to calculate the surface area and volume for each crystal. The appropriate mensuration formulas are used for each crystal shape, with assumptions listed in Table 4. For example, assumptions are made about the hollowness of diamond-dust columns and the individual bullets of a bullet cluster, which affect their computed surface area (A) and volume (V).

The size distributions for each crystal type are generated by first representing the nonspherical ice particles by a collection of “equivalent” spheres. Spheres with the same volume-to-area ratio (V/A) as the crystals are used here because of the importance of V/A in calculating radiative fluxes and heating rates in atmospheric radiation models. Grenfell and Warren (1999) have shown that equal V/A spheres provide a good approximation for the extinction efficiency, the single-scattering albedo, and the asymmetry parameter over a wide range of wavelengths from the ultraviolet through the infrared. A single nonspherical particle is represented by a collection of independent spheres that has the same total surface area and total volume as the nonspherical particle. Equations (1) and (2) from Grenfell and Warren (1999) give the equal V/A radius, r_{VA} , and the number of spheres per crystal, n_s , as

$$r_{VA} = 3\frac{V}{A} \quad \text{and} \quad (1)$$

$$n_s = \frac{3V}{4\pi r_{VA}^3}, \quad (2)$$

where V and A are the volume and surface area of the nonspherical particle, respectively.

Some authors (e.g., Fu et al. 1999) prefer to use projected area P instead of total surface area A when computing the equivalent radius. For convex particles the two methods give exactly the same value of r_{VA} , because $A = 4P$ for all convex shapes (Vouk 1948), and so $r_{VA} = 3V/A = 3V/4P$. However, for crystals with concavities, we think it is probably important to count the inner surfaces when using spheres to mimic such a crystal, because scattering can occur at those, as well as at the external, surfaces. For this reason we prefer to define r_{VA} in terms of total surface area instead of projected area, so that it can be applied to all nonspherical crystals, not just convex shapes.

As mentioned in section 2b(1), hexagonal plates often had unequal sides. We believe that this is probably true for columns as well, although this asymmetry was not measured. Because the columns were assumed to have all sides equal, but were probably asymmetric and lying on their broad side, our estimates of the surface area and volume are both biased high. Laboratory experiments by Bailey and Hallett (2000) and Kajikawa et al. (1980) find that the width of the broad sides is typically 1.6–2.5 times the width of the narrow sides. These biases tend to cancel somewhat when calculating the V/A ratio, but r_{VA} is still probably biased high by 15%–50%.

The equal V/A specification for equivalent spheres was validated by Mahesh et al. (2001, their Fig. 16). They inferred effective radii from ground-based remote sensing using the infrared emission spectrum, and compared these radii to those of crystals photographed on the collection slide. Three specifications of equivalent sphere were tried: equal area, equal volume, and equal V/A ; the equal V/A specification clearly agreed best with the radii inferred from remote sensing.

It is interesting to compare the equal V/A spheres that represent a solid column with those that represent a hollow column of the same outer dimensions. Consider a solid column that has the average dimensions of diamond-dust columns observed at the South Pole: $c = 61 \mu\text{m}$, $2a = 13 \mu\text{m}$. Also, consider a hollow column with the same outer dimensions, but with a large air pocket of dimensions $45 \mu\text{m} \times 10 \mu\text{m}$. The surface area of the hollow column is approximately 1.3 times that of the solid column, while its volume is about 80% of the solid column. The solid column is represented by about 3.5 equal V/A spheres with $r_{VA} = 7.7 \mu\text{m}$, while the hollow column is represented by 44 spheres with $r_{VA} = 2.7 \mu\text{m}$.

For radiative transfer calculations, the most important

single measure of a size distribution is the area-weighted mean radius, or “effective radius,” r_{eff} , which was defined for spheres by Hansen and Travis (1974):

$$r_{\text{eff}} = \frac{\int r^3 n(r) dr}{\int r^2 n(r) dr}. \quad (3)$$

For each crystal, we compute r_{VA} and n_s from (1) and (2), and then compute r_{eff} for a size distribution from (3), using $r = r_{VA}$ and $n(r) = n_s$.

The resolution of the photomicrographs allows measurements down to about 2–3 μm , which is less than the sizing limits of most conventional particle measurement probes (Lawson et al. 2001; Gultepe et al. 2001). Because the dimensions of small particles are measured directly in this study, our calculations of the effective radius of size distributions are more accurate than those that must assume the distribution of small particles. Of course, we intentionally excluded the micrometer-size “breath crystals” from our statistics because they are artifacts.

4. Results

a. Summary of microphysical parameters

Table 2 gives the means and extremes of the crystal dimensions. The longest dimension was 1000 μm , the c axis of the long diamond-dust column in Fig. 2b. The smallest dimension was 2 μm , which occurred for solid columns. The smallest mean dimension was the width of solid columns and the thickness of plates, 13 μm ; the largest mean was the c axis of the bullets in bullet clusters, 243 μm .

Figure 4 displays the dimensions of diamond-dust ice crystals, plotted as both the crystal length (c) versus crystal width ($2a$), and as a histogram of aspect ratios ($c/2a$). By definition, columns have an aspect ratio greater than 1, while plates have $c/2a < 1$. Shimizu (1963) first demonstrated the existence of long prisms, now sometimes called Shimizu crystals, for which $c/2a > 5$. Figure 4b shows that these crystals are quite common. The crystal with the maximum value of $c/2a$ (about 100) for the entire 1992 dataset is shown in Fig. 2b. The values of $2a$ for diamond dust range from 2 to 158 μm ; the values of c range from 3 to 1000 μm .

Figure 4 shows a paucity of equidimensional crystals ($c \approx 2a$). This is not an artifact of the process of sizing the crystals due to the choice of whether a crystal is a column or a plate, or due to how the plates with one measurable dimension are handled. It is rather a real feature that suggests that diamond-dust crystals are rarely equidimensional.

Figure 5 shows the dimensions of blowing-snow particles. By definition, the semimajor axis a is longer than the semiminor axis b . Blowing-snow particles are small,

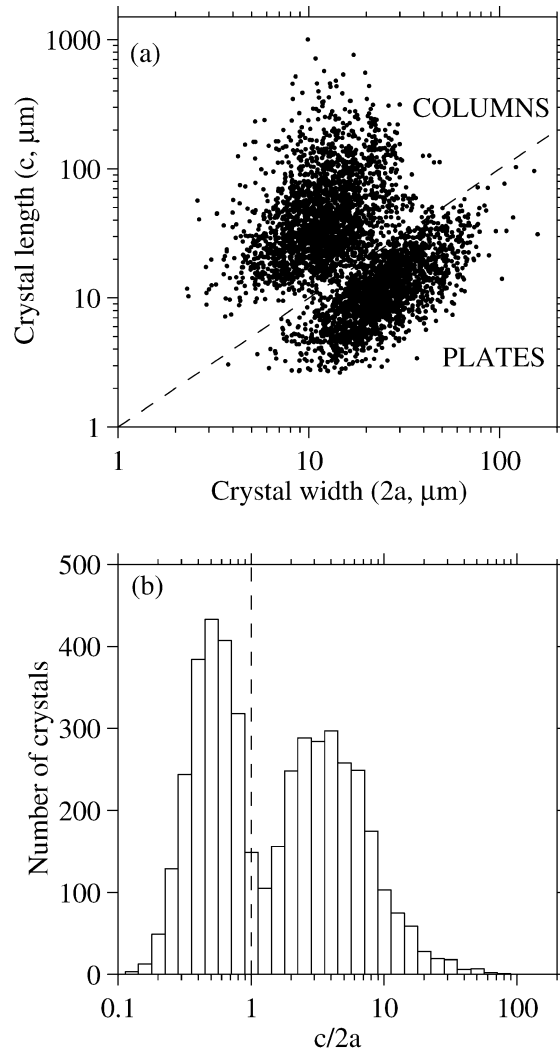


FIG. 4 (a) Dimensions of solid columns and plates and (b) frequency distribution of aspect ratios ($c/2a$). In (a), the dashed line with slope of 1 designates the boundary between plates ($c/2a \leq 1$) columns ($c/2a > 1$). Long-prism columns were defined by Shimizu (1963) as those having $c/2a > 5$. There are 4508 crystals plotted here.

with semidimensions between 1 and 65 μm . The average values of $2a$ and $2b$ are 19 and 15 μm . The average aspect ratio (a/b) is 1.4 for the crystals shown in Fig. 5.

Figures 6–8 show the size distributions of each crystal type; Fig. 9 shows the distributions of the three major categories of ice crystals. These figures are plotted on a semilog graph because the size distributions sometimes resemble lognormal distributions (Reist 1993). The geometric mean radius (r_g) and geometric standard deviation (σ_g) are listed for only those size distributions that appear lognormal: solid columns and plates in Fig. 6, blowing snow in Fig. 7, and the three major categories in Fig. 9.

Table 5 gives the effective radius for each crystal type and also for each of the three major categories of crystals. The effective radius for diamond dust is 12.2 μm .

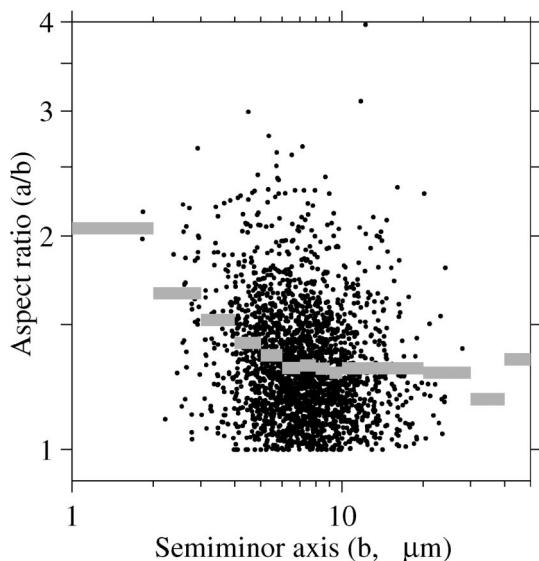


FIG. 5. Dimensions of blowing-snow particles, plotted as the aspect ratio (a/b) vs the semiminor axis b . Only one-fifth of the blowing-snow particles are plotted for clarity. The gray, horizontal lines represent the average aspect ratios for all blowing-snow particles within that size bin; all of the particles were used to compute these averages. The vertical axis is plotted as the fifth root of the aspect ratio to expand the scale at small values.

This is a weighted average of columns ($r_{\text{eff}} = 10.1 \mu\text{m}$) and plates ($r_{\text{eff}} = 15.1 \mu\text{m}$). The effective radius for hollow columns ($r_{\text{eff}} = 6.4 \mu\text{m}$) is much smaller than that for solid columns, as discussed above, but hollow columns are very rare. The effective radius for blowing snow is $11 \mu\text{m}$. Snow grains are larger than both diamond dust and blowing snow, with an effective radius of $24 \mu\text{m}$. Snow-grain columns are much larger ($r_{\text{eff}} = 67 \mu\text{m}$) than both sector-plate ($12 \mu\text{m}$) and bullet ($25 \mu\text{m}$) clusters, because the sector plates in clusters are thin (assumed $10 \mu\text{m}$) and bullets are hollow (see assumptions in Table 4).

Figure 10 shows the distribution of daily effective radii for each of the 84 days that were sampled. The most probable effective radius is about $11 \mu\text{m}$ for any given day in winter, because this is roughly the effective radius of both blowing snow and diamond dust. There were a few days when larger particles dominated; the images for these days were largely populated with snow grains.

b. Correlation with meteorological conditions

Attempts were made to correlate the aspect ratio of diamond dust ($c/2a$) and the semimajor axis of blowing snow with meteorological conditions using data from SPWO. Hourly measurements of the 2-m air temperature T_s , and 10-m wind speed u and direction ϕ , were obtained from SPWO. These data were averaged over the approximate exposure times of the microscope slide to the atmosphere to yield meteorological values that

pertain to each photomicrograph. The surface temperatures ranged from about -75° to -35°C , while the wind speeds ranged from about 2 to 11 m s^{-1} .

Radiosondes were launched by the SPWO once per day during winter. Each temperature profile was corrected for thermal lag of the radiosonde's thermistor by the method of Mahesh et al. (1997). A surface-based temperature inversion was present every day throughout the winter, although it varied in strength. The corrected radiosonde profiles were used to generate several measures of the surface-based temperature inversion: 1) the inversion-top temperature T_i , the maximum temperature in the lowest 1200 m of the atmosphere; 2) the inversion height h_i , the height of the maximum temperature; 3) the inversion strength ($T_i - T_s$), where T_s is taken at the time of the radiosonde launch; and 4) the inversion lapse rate Γ , the inversion strength divided by the inversion height. A typical wintertime inversion for 1992 had a strength of 20 K with a height of only 500 m, yielding a lapse rate of -40 K km^{-1} ; the range of lapse rates was from about -10 to -150 K km^{-1} . The inversion-top temperatures ranged from -50° to -25°C , while the inversion heights ranged from about 200 to 1150 m above the surface.

We suspect that a strong near-surface humidity inversion exists, but the humidity sensors used on routine radiosondes are unable to measure the water vapor profile accurately because the sensors have response times of several minutes at these temperatures. The humidity values at the top of the inversion are probably critical to the formation of diamond dust.

Table 6 lists the slopes of the correlations of particle size with various meteorological conditions; the correlation coefficients (r^2) are listed in parentheses. None of the correlations with diamond dust are significant. Two of the largest slopes, although not significant, indicate a decrease in particle size of both diamond dust and blowing snow with increasing wind speed. The only significant correlation for the semimajor axis of blowing snow is with the inversion-top temperature ($r^2 = 0.31$), although there is no apparent reason for this. Because of the weak correlations, the size distributions presented in section 4 can be expected to represent conditions throughout the entire Antarctic winter.

5. Discussion

a. Diamond dust

Most of the diamond-dust crystals have simple shapes: solid plates or columns with few inclusions of air. These are the shapes to be expected when the growth is slow because of low excess water vapor density (Fletcher 1970, his Fig. 5.6), a condition that always holds on the Antarctic Plateau, especially in winter. These simple shapes resulting from slow growth are what are required to generate the full set of halo patterns, which are, therefore, observed with far greater frequen-

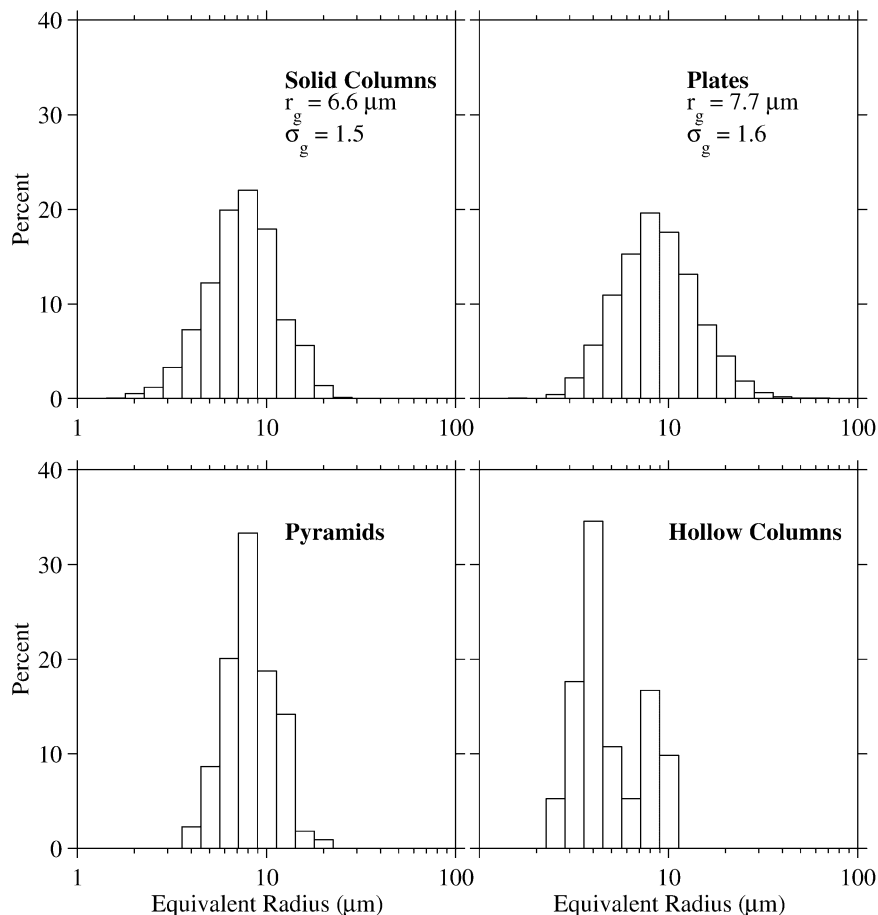


FIG. 6. Size distributions of the four different types of diamond dust. The geometric mean radius (r_g) and standard deviations (σ_g) are listed for solid columns and plates only, because they appear to have lognormal size distributions. The histograms show the percent occurrence of equivalent spheres (n_s).

cy on the Antarctic Plateau than anywhere else on the earth (Tape 1994).

The crystal shapes we observed for wintertime diamond dust are the same as those reported for summertime crystals by Tape (1994), Kikuchi and Hogan (1979), and others. However, the crystals are smaller in winter. We have taken the c and a axis lengths reported in Fig. 7 of Kikuchi and Hogan (1979) and converted them to equal V/A radii r_{VA} , using Eq. (1). Their summertime diamond dust had $r_{VA} = 17.5 \mu\text{m}$, larger than the $12.2 \mu\text{m}$ we find in winter. This is to be expected because the higher temperatures of summer imply a much greater water vapor density. At the typical summer temperature of -30°C , the saturation vapor pressure over ice is a factor of 40 larger than that at the typical winter temperature of -60°C . Crystals of $r_{VA} = 12 \mu\text{m}$ fall very slowly, and they can grow by vapor deposition as they fall, but in winter they can fall all the way to the surface without growing much because the water vapor density is so low.

Past investigations have shown that the preference for

“axial” growth (in the c direction) versus “lateral” growth (in the basal plane) is determined by temperature. It used to be thought that, at about -25°C , only axial growth occurs, resulting in columns (Fletcher 1970; Kobayashi 1958, 1967). However, there is now abundant evidence, reviewed by Bacon et al. (2003), that both plates and columns can occur at low temperatures. We often found both plates and columns on days when temperatures throughout the troposphere were below -40°C , supporting the conclusion of Bacon et al. that factors other than temperature often determine whether a or c axis growth will dominate.

The extremely long “Shimizu” crystals were seen only occasionally, and on one day (19 August) the collection consisted entirely of long prisms (Fig. 2e). Examination of the weather reports for this day revealed nothing unusual, so we have not identified a meteorological condition conducive to the formation of long prisms. Perhaps the method of nucleation, rather than the environment of growth, is the determining factor.

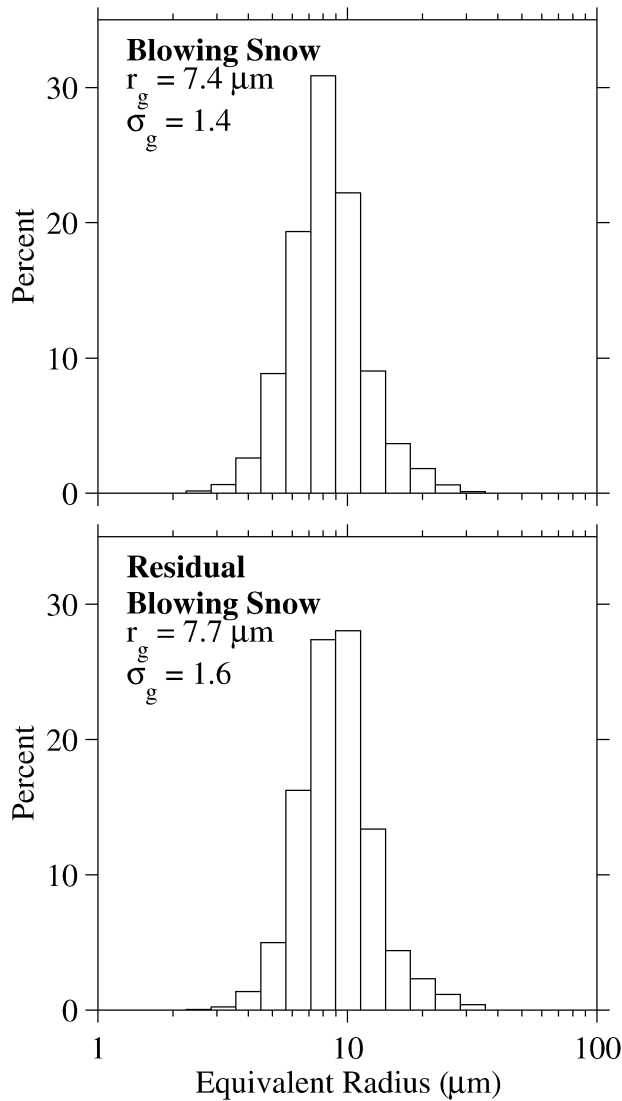


FIG. 7. Size distributions of blowing snow. The geometric mean radii (r_g) and standard deviations (σ_g) are listed, because the distributions appear to be lognormal. The histograms show the percent occurrence of equivalent spheres (n_s).

No investigation of ice nucleation was carried out in this study.

The frequent formation of diamond dust in the near-surface atmosphere suggests the possibility for studying ice-cloud processes at the surface. However, our measurements may not be relevant to cirrus clouds because the dominant formation processes are different. Cirrus clouds usually experience greater turbulence and faster crystal growth. The crystals in cirrus (e.g., Ono 1969; Heymsfield 1975; Heymsfield and Platt 1984; Lawson et al. 1998), particularly those at warmer temperatures than those of this study, have more irregular shapes (such as bullet clusters), and more closely resemble the snow grains we sampled than the diamond dust.

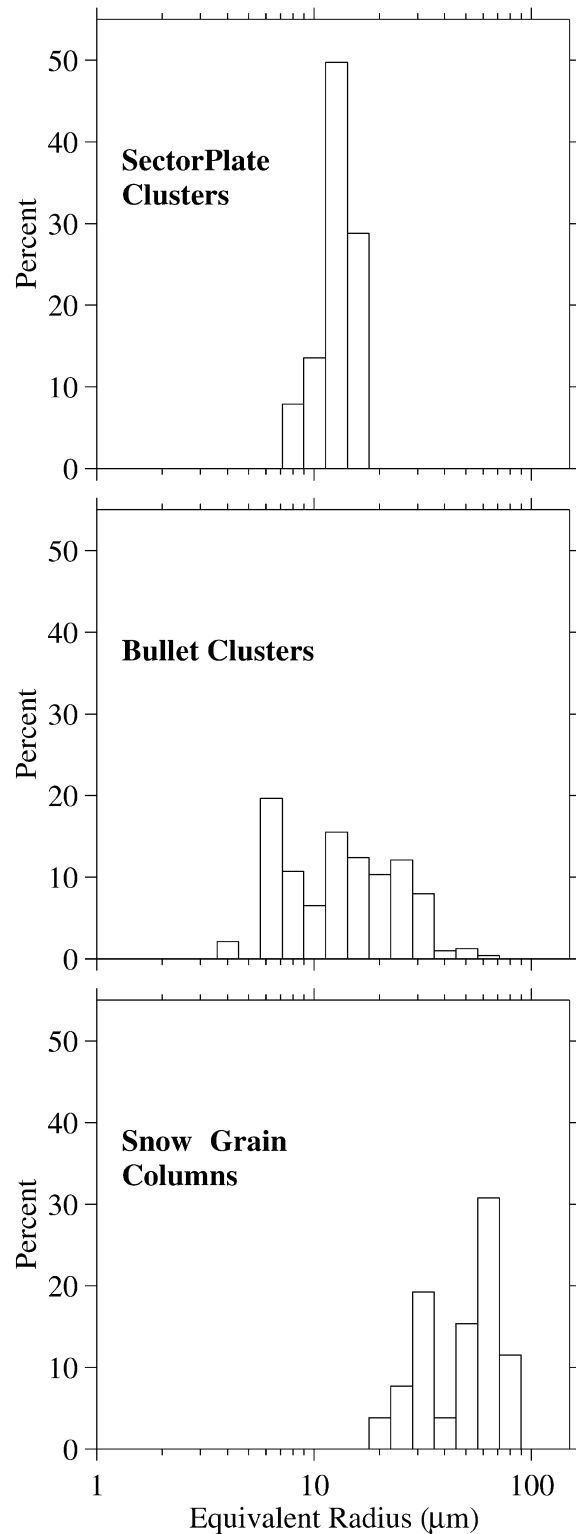


FIG. 8. Size distributions of the three different types of snow grains. The histograms show the percent occurrence of equivalent spheres (n_s).

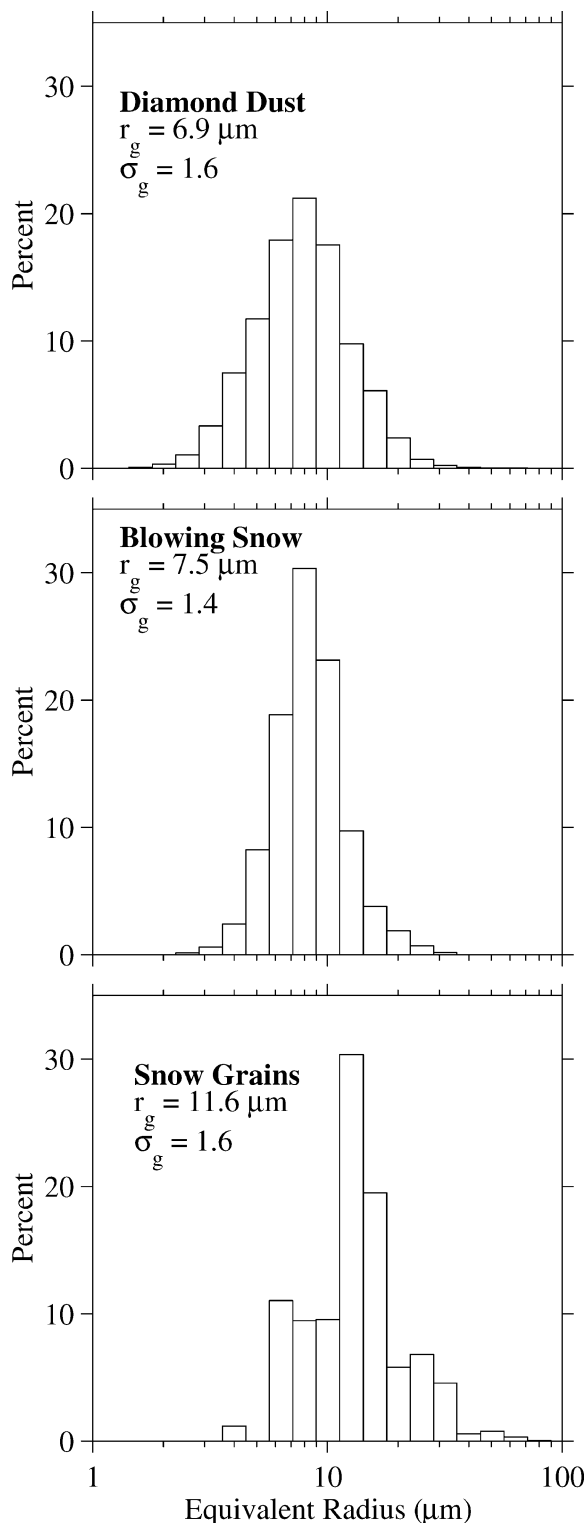


FIG. 9. Size distributions of the three main types of wintertime ice crystals. The geometric mean (r_g) and standard deviations (σ_g) are listed for each distribution. The histograms show the percent occurrence of equivalent spheres (n_s).

TABLE 5. Effective radius for the individual crystal types and the three major categories of crystals.

Crystal type	Effective radius, r_{eff} (μm)
Diamond dust	12.2
Solid columns	10.1
Plates	15.1
Pyramids	9.4
Hollow columns	6.4
Blowing snow	11.0
Blowing snow	10.8
Residual blowing snow	11.9
Snow grains	23.6
Sector-plate clusters	11.9
Bullet clusters	25.2
Snow-grain columns	67.0

b. Blowing snow

Blowing snow is an important atmospheric phenomenon in the polar regions. In addition to redistributing precipitation, blowing snow can affect the longwave radiation budget (Yamanouchi and Kawaguchi 1985). It also has practical effects on astronomical “seeing” and on ice-core stratigraphy.

Blowing snow undergoes a seasonal cycle in frequency of occurrence, particle size, and vertical extent. At the South Pole, surface snow begins to be lifted by wind at a speed of about 7 m s^{-1} . Blowing snow often continues to be observed for 1–2 days after the wind speed drops below 7 m s^{-1} , because of saltation (Schmidt 1982); this is the “residual blowing snow” shown in Tables 2, 3, and 5, and in Fig. 7. However,

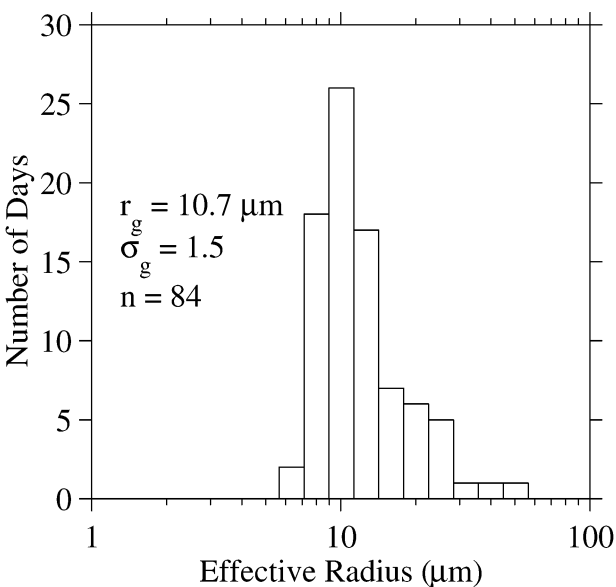


FIG. 10. An effective radius was determined for the entire assemblage of crystals on each day. The frequency distribution of the daily effective radii is plotted here.

TABLE 6. Correlations of the sizes of diamond-dust ice crystals and blowing-snow particles with boundary layer meteorological parameters at South Pole Station, 1992. The slopes of the least squares fits between the particle sizes and each meteorological parameter are listed. The correlation coefficients (r^2) are listed in parentheses.

Meteorological parameters	Measurement interval	Diamond dust	Blowing snow
Surface temperature	-73° to -40°C	$-0.032 \mu\text{m } ^\circ\text{C}^{-1}$ (0.01)	$+0.25 \mu\text{m } ^\circ\text{C}^{-1}$ (0.15)
Inversion-top temperature	-51° to -27°C	$+0.018 \mu\text{m } ^\circ\text{C}^{-1}$ (0.00)	$+0.46 \mu\text{m } ^\circ\text{C}^{-1}$ (0.31)
Inversion strength	5 to 32 K	$+0.083 \mu\text{m K}^{-1}$ (0.03)	$-0.0035 \mu\text{m K}^{-1}$ (0.00)
Lapse rate	-154 to -8 K km^{-1}	$-0.0018 \mu\text{m (K km}^{-1})^{-1}$ (0.00)	$-0.00066 \mu\text{m (K km}^{-1})^{-1}$ (0.00)
Inversion height	196 to 1162 m	$+0.0011 \mu\text{m m}^{-1}$ (0.01)	$+0.0010 \mu\text{m m}^{-1}$ (0.00)
Wind speed	1.8 to 11.3 m s^{-1}	$-0.34 \mu\text{m (m s}^{-1})^{-1}$ (0.07)	$-0.39 \mu\text{m (m s}^{-1})^{-1}$ (0.04)
Wind direction	10° to 350°	$-0.0080 \mu\text{m (}^\circ)^{-1}$ (0.02)	$-0.0075 \mu\text{m (}^\circ)^{-1}$ (0.01)

the threshold wind speed for dislodging snow grains from the surface is variable. We observed on one occasion at the South Pole (in summer, not during the time we collected crystals) that a full day of 10 m s^{-1} wind did not result in blowing snow, because the snow surface had previously been cemented by rime a few days earlier when a fog of supercooled water droplets passed over the surface.

The blowing snow extends to much greater heights in winter than in summer. In summer it is confined to the lowest few meters, but in winter it greatly exceeds the 21-m height of the meteorological tower at South Pole Station. It is more difficult to dislodge snow grains from the surface in summer, because soon after falling they form bonds by sintering (LaChapelle 1969). Furthermore, the individual particles of blowing snow are probably smaller in winter than in summer (because the precipitation crystals, which are their ultimate source, are smaller) and can, thus, be lofted higher. In addition, the accumulation rate at South Pole is significant (about 20 cm yr^{-1}). Gow (1965) presented evidence that the blowing snow being lifted into the air during winter most likely fell during that same winter.

6. Conclusions

Nine different types of ice crystals were identified and sized for the Antarctic winter of 1992. These crystals are categorized into three main groups: diamond dust, blowing snow, and snow grains. Wintertime diamond-dust ice crystals, which are primarily solid columns and plates, have a wide range of aspect ratios. Blowing-snow particles are small and round, with aspect ratios near 1. Snow grains, which precipitate from clouds, have much larger surface area and volume than either diamond dust or blowing snow, but occur much less frequently. The effective radii for diamond dust, blowing snow, and snow grains are 12, 11, and $24 \mu\text{m}$, respectively. Although diamond-dust particles are much

longer than blowing-snow particles, their short dimensions are similar, and it is their short dimensions that primarily determine r_{VA} .

The aspect ratio of diamond-dust ice crystals, and the size of blowing-snow particles, are uncorrelated with meteorological conditions measured at the surface or within the near-surface temperature inversion. This suggests that the size distributions presented here may be used to represent the entire antarctic winter. Size distributions are presented for each of the nine crystal types as well as the three main categories of crystals. Geometric mean radii and standard deviations are given for the predominant crystal types and the three main categories. The size distribution of effective radii for each day is presented. The most probable effective radius in wintertime is about $11 \mu\text{m}$.

Acknowledgments. Betty Carlisle, the South Pole physician for 1992, allowed us to use the microscope and gridded slide from her clinic for this experiment. Bert Davis suggested the use of the xv and IPW software packages and helped us to apply them to this study. Victoria Campbell from Antarctic Support Associates supplied the meteorological data. Ash Mahesh assisted with the initial data analysis. Discussions with Marcia Baker, Charles Knight, Andrew Heymsfield, Brian Swanson, and Matthew Bailey, and the comments of one anonymous reviewer, have been helpful. This research was supported by NSF Grants OPP-91-20380, OPP-94-21096, and OPP-97-26676 to the University of Washington, and by ATM-98-20043 to the University of Wisconsin—Madison.

REFERENCES

- Asuma, Y., Y. Inoue, K. Kikuchi, N. Sato, and T. Hayasaka, 2000: Wintertime precipitation behavior in the western Canadian Arctic region. *J. Geophys. Res.*, **105**, 14 927–14 939.
- Bacon, N. J., M. B. Baker, and B. D. Swanson, 2003: Initial stages

- in the morphological evolution of vapor grown ice. A laboratory investigation. *Quart. J. Roy. Meteor. Soc.*, **129**, 1903–1928.
- Bailey, M., and J. Hallett, 2000: Nucleation, growth, and habit distribution of cirrus type crystals under controlled laboratory conditions. *Proc. 13th Int. Conf. on Clouds and Precipitation*, Reno, NV, International Commission on Clouds and Precipitation (ICCP) of the International Association of Meteorology and Atmospheric Sciences (IAMAS), 629–632.
- Blanchet, J.-P., and E. Girard, 1994: Arctic greenhouse cooling. *Nature*, **371**, 383.
- Chen, J.-P., G. M. McFarquhar, A. J. Heymsfield, and V. Ramanathan, 1997: A modeling and observational study of the detailed microphysical structure of tropical cirrus anvils. *J. Geophys. Res.*, **102**, 6637–6653.
- Fletcher, N. H., 1970: *The Chemical Physics of Ice*. Cambridge University Press, 271 pp.
- Fu, Q., W. B. Sun, and P. Yang, 1999: Modeling of scattering and absorption by nonspherical cirrus ice particles at thermal infrared wavelengths. *J. Atmos. Sci.*, **56**, 2937–2947.
- Girard, E., and J.-P. Blanchet, 2001a: Microphysical parameterization of arctic diamond dust, ice fog, and thin stratus for climate models. *J. Atmos. Sci.*, **58**, 1181–1198.
- , and —, 2001b: Simulation of arctic diamond dust, ice fog, and thin stratus using an explicit aerosol–cloud–radiation model. *J. Atmos. Sci.*, **58**, 1199–1221.
- Gow, A., 1965: On the accumulation and seasonal stratification of snow at the South Pole. *J. Glaciol.*, **5**, 467–477.
- Grenfell, T. C., and S. G. Warren, 1999: Representation of a nonspherical ice particle by a collection of independent spheres for scattering and absorption of radiation. *J. Geophys. Res.*, **104**, 31 697–31 709.
- Gultepe, I., G. A. Isaac, and K. B. Strawbridge, 2001: Variability of cloud microphysical and optical parameters obtained from aircraft and satellite remote sensing measurements during RACE. *Int. J. Climatol.*, **21**, 507–525.
- Hahn, C. J., S. G. Warren, and J. London, 1995: The effect of moonlight on observation of cloud cover at night, and application to cloud climatology. *J. Climate*, **8**, 1429–1446.
- Hansen, J. E., and L. D. Travis, 1974: Light scattering in planetary atmospheres. *Space Sci. Rev.*, **16**, 527–610.
- Hatanaka, M., S. Kimura, Y. Yoshida, M. Wada, and N. Hirasawa, 1999: Snow particle size distributions at Syowa Station, Antarctica in 1988. *Polar Meteor. Glaciol.*, **13**, 148–156.
- Heymsfield, A., 1975: Cirrus uncinus generating cells and the evolution of cirriform clouds. Part I: Aircraft observations of the growth of the ice phase. *J. Atmos. Sci.*, **32**, 799–808.
- , and C. M. R. Platt, 1984: A parameterization of the particle size spectrum of ice clouds in terms of the ambient temperature and the ice water content. *J. Atmos. Sci.*, **41**, 846–855.
- Hogan, A. W., 1975: Summer ice crystal precipitation at the South Pole. *J. Appl. Meteor.*, **14**, 246–249.
- Kajikawa, M., K. Kukuchi, and C. Magono, 1980: Frequency of occurrence of peculiar shapes of snow crystals. *J. Meteor. Soc. Japan*, **58**, 416–421.
- Kikuchi, K., 1972: Sintering phenomenon of frozen cloud particles observed at Syowa Station, Antarctica. *J. Meteor. Soc. Japan*, **50**, 131–135.
- , and A. W. Hogan, 1979: Properties of diamond dust type ice crystals observed in summer season at Amundsen-Scott South Pole Station, Antarctica. *J. Meteor. Soc. Japan*, **57**, 180–190.
- Kobayashi, T., 1958: On the habit of snow crystals artificially produced at low pressures. *J. Meteor. Soc. Japan*, **36**, 193–208.
- , 1967: On the variation of ice crystal habit with temperature. *Physics of Snow and Ice*, H. Oura, Ed., Bunyuido, 95–104.
- Korolev, A. V., G. A. Isaac, and J. Hallett, 1999: Ice particle habits in Arctic clouds. *Geophys. Res. Lett.*, **26**, 1299–1302.
- LaChapelle, E. R., 1969: *Field Guide to Snow Crystals*. University of Washington Press, 101 pp.
- Lawson, R. P., A. J. Heymsfield, S. M. Aulenbach, and T. L. Jensen, 1998: Shapes, sizes and light scattering properties of ice crystals in cirrus and a persistent contrail during SUCCESS. *Geophys. Res. Lett.*, **25**, 1331–1334.
- , B. A. Baker, C. G. Schmitt, and T. L. Jensen, 2001: An overview of microphysical properties of Arctic clouds observed in May and July 1998 during FIRE ACE. *J. Geophys. Res.*, **106**, 14 989–15 014.
- Lubin, D., B. Chen, D. H. Bromwich, R. C. J. Somerville, W.-H. Lee, and K. M. Hines, 1998: The impact of Antarctic cloud radiative properties on a GCM climate simulation. *J. Climate*, **11**, 447–462.
- Mahesh, A., V. P. Walden, and S. G. Warren, 1997: Radiosonde temperature measurements in strong inversions: Correction for thermal lag based on an experiment at the South Pole. *J. Atmos. Oceanic Technol.*, **14**, 45–53.
- , —, and —, 2001: Ground-based infrared remote sensing of cloud properties over the Antarctic Plateau. Part II: Cloud optical depth and particle sizes. *J. Appl. Meteor.*, **40**, 1279–1294.
- Ohtake, T., 1978: Atmospheric ice crystals at the South Pole in summer. *Antarct. J. U.S.*, **13**, 174–175.
- , and T. Yogi, 1979: Winter ice crystals at the South Pole. *Antarct. J. U.S.*, **14**, 201–203.
- Ono, A., 1969: The shape and riming properties of ice crystals in natural clouds. *J. Atmos. Sci.*, **26**, 138–147.
- Pruppacher, H. R., and J. D. Klett, 1978: *Microphysics of Clouds and Precipitation*. Reidel, 714 pp.
- Reist, P. C., 1993: *Aerosol Science and Technology*. 2d. ed. McGraw-Hill, 379 pp.
- Schmidt, R. A., 1982: Properties of blowing snow. *Rev. Geophys. Space Phys.*, **20**, 39–44.
- Schutz, B. E., 1998: *Spaceborne Laser Altimetry: 2001 and Beyond. Extended Abstracts, WEGENER-98*, Honefoss, Norway, International Association of Geodesy (IAG), 1–4.
- Shimizu, H., 1963: “Long prism” crystals observed in the precipitation in Antarctica. *J. Meteor. Soc. Japan*, **41**, 305–307.
- Smiley, V. N., B. M. Whitcomb, B. M. Morley, and J. A. Warburton, 1980: Lidar determinations of atmospheric ice crystal layers at South Pole during clear-sky precipitation. *J. Appl. Meteor.*, **19**, 1074–1090.
- Tape, W., 1994: *Atmospheric Halos*. Antarctic Research Series, Vol. 64, Amer. Geophys. Union, 143 pp.
- Vouk, V., 1948: Projected area of convex bodies. *Nature*, **162**, 330–331.
- Yamanouchi, T., and S. Kawaguchi, 1985: Effects of drifting snow on surface radiation budget in the katabatic wind zone, Antarctica. *Ann. Glaciol.*, **6**, 238–241.